Systematic Effects of Randomness in Radiative Transfer

WILLIAM I. NEWMAN

Departments of Earth and Space Sciences, Astronomy, and Mathematics, University of California, Los Angeles, California

JEFFREY K. LEW, GEORGE L. SISCOE, AND ROBERT G. FOVELL

Department of Atmospheric Sciences, University of California Los Angeles, Los Angeles, California

(Manuscript received 18 November 1993, in final form 20 June 1994)

ABSTRACT

In this paper, the authors show how the variability of the water content in individual clouds, the complexity of individual cloud structure, and the lateral and vertical heterogeneity of the distribution of individual clouds can produce *systematic* effects in the inversion of intensity distributions and the inference of source functions and the vertical temperature profile. This is possibly very significant, even in simple applications of radiative transfer theory where multiple scattering is not very important, in light of the randomness in the water vapor content and geometry associated with the microphysics of clouds. A practical procedure is provided to quantify this effect and to obtain, in certain circumstances, an improved estimate of the vertical temperature profile.

1. Introduction

As our understanding of the microphysics of clouds has grown, so too has our appreciation of their complex nature. Convection in a wet-adiabatic environment gives rise to cumulus clouds, for example, whose geometry is the by-product of complicated dynamics and competition between wet and dry parcels of air. The spatial variability of cloud microstructure is well established. In a given cloud, the liquid water contents tend to be higher in stronger updrafts, which vary in intensity between the edges and the center of a developing cumulus cell (e.g., Warner 1969; Heymsfield and Musil 1982). Meanwhile, the entrainment along the edges and tops of rising thermals serves to decrease the liquid water content and water vapor mixing ratios in these areas, leading to significant horizontal, vertical, and temporal nonuniformities within a single cumulus cloud. Indeed, often one "single" cumulus or stratocumulus cloud of large areal extent can be composed of several convective cells of complex spatial structure and temporal evolution characteristics. These cells can be overlapping (as observed along some line of sight) and can be in various stages of development, thus producing a complicated pattern of liquid water content and water vapor (Johnson 1957). If we assume that the air is always at or near water saturation, then the nonuniformities in the cloud dynamical structure will lead to spatial variations in temperature, which will then produce nonuniformities in the horizontal structure of the vertically integrated water vapor content. The outcome of these considerations is that the liquid water content and geometry of individual clouds will generally be very complex.

Stratus clouds usually have more horizontally homogeneous vertical wind fields than cumulus clouds; therefore, one would expect the distribution of liquid water to be more uniform at a single altitude. Aircraft measurements by Telford and Wagner (1981) show that even stratus clouds have some finescale structure, particularly near the top of the cloud, where a stratus cloud may have a "bubbly" appearance, similar to weak cumuliform convection. Orographic clouds also appear to be horizontally homogeneous like stratus clouds. However, observations of Hawaiian orographic clouds show that while the orographic cloud deck visually appears stratiform from above, there may be cumuliform cells pushing into the main cloud from below, giving the cloud a highly variable liquid water content and water vapor structure (Squires and Warner 1957).

In Fig. 1, we reproduce from Slingo et al. (1982) the time series of the integrated liquid water paths derived from ground-based microwave radiometer measurements of the sky brightness temperature at the zenith. The vertical axis, that is, the liquid water path, is directly proportional to the optical depth, while the horizontal axis indicates the (relative) time in hours of observation. The variability seen in these measurements is a direct indication of the randomness present

Corresponding author address: Dr. William I. Newman, Department of Earth and Space Sciences, University of California, 3806 Geology Building, Los Angeles, CA, 90024-1567.

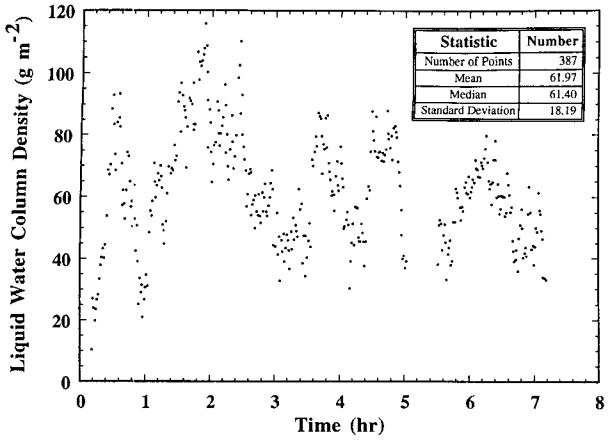

FIG. 1. Data from Slingo et al. (1982) showing a time series of the integrated liquid water paths derived from microwave radiometer data. The points are one-minute averages, and the axes describe the relative time in hours (horizontal) and the liquid water path (g m^{-2}) (vertical).

in the distribution of liquid water, the geometry of the individual clouds wherein the water is situated, and the lateral (and vertical) placement of the clouds themselves. (Slingo et al. noted variability on both mesoscale and microscale, but the possibility of variations on all scales remains.) In traditional treatments of radiative transfer theory (e.g., Houghton 1988), randomness associated with these physical effects is not included in the formulation of the theory. The variation of the optical depth relative to its mean is 30%. In radiative transfer theory, this variability has until now been ignored! These observations are particularly significant since, as they refer to water in clouds, they describe one of the principal components in the atmospheric "greenhouse"—any systematic effects associated with the treatment of this data will necessarily have a substantial influence on our interpretation of the greenhouse effect. Could this observed variability have any significant and possibly *systematic* effect on radiative transfer and influence conclusions then drawn in weather prediction and climatic change?

The geometry of individual clouds has attracted some attention in recent years, although the more significant quantitative issue is the variability of water droplets within clouds and the horizontal placement of individual clouds. The corrugated texture of clouds is now recognized as an indication of statistical scaling properties: magnified images of portions of a cloud have the same texture or statistical properties as the original cloud. The corrugated texture, for example, of the outline of a cloud indicates that it is not sufficient to think of the periphery as being one-dimensional, but that the cloud in part intrudes upon the second dimension. Hence, the notion of a fractal (or "fractional") dimension that would describe the cloud outline as having a dimension larger than 1 but less than 2, where higher numbers are reserved for more corrugated geometry. Lovejoy (1982) and Carter and Siscoe (1987), among others, observed that the areal and vertical projections of clouds possess fractal scaling properties, with fractal dimensions of 1.33 and 1.07, respectively. Hentschel and Procaccia (1984) modeled the lateral dynamics in terms of turbulent and diffusive processes and suggested that these would produce the observed scaling properties while Mandelbrot (1988) proposed that the difference in the fractal dimensions was due to the inhibiting role of gravity in determining vertical structure; hence, the fractal dimension of the vertical profile is reduced. Prevailing models of entrainment (e.g., see Rogers and Yau 1989; Cotton and Anthes 1989) do not reproduce these geometrical effects, although recent efforts by Bretherton (1990) show some hint of this. Meanwhile, the more important question of liquid water distribution and the distribution of assemblies of clouds has not yielded any fundamental simplifications and remains a central problem among cloud microphysicists. The essential point here is that there is demonstrable evidence that many different sources of randomness substantially influence quantities of direct relevance to radiative transfer and possibly, therefore, to meteorological and climatological questions.

The subject of randomness in radiative transfer has been a vexing one for atmospheric scientists for many years. For the analytic demonstration and analysis of data presented here, it is not necessary to invoke the elaborate machinery for this problem that has evolved over many years. However, it is useful to enumerate some of the important contributions in this area. Perhaps the most comprehensive of these is the book by Pomraning (1991). A variety of results that have emerged during investigations of multiple scattering—a process we do not need to invoke to explain our observations—can be found in Stephens (1988a,b) as well as in Cahalan (1989). Other treatments of nonlinearity in the attenuation of the intensity may be found in Davis et al. (1991b), Stephens et al. (1991), Barker (1993), and Evans (1993). Other parameterizations, including the notion of "packing factor" in conservatively scattering media, can be found in Davis et al. (1991a). This latter reference observes that Jensen's inequality is satisfied in numerical simulations; we will later show that Jensen's inequality plays a major role in radiative transfer. Finally, Davis et al. (1990) provide a comprehensive literature of the subject of randomness (particularly in simulations and in models) in atmospheric radiative transfer.

In this paper, we will show using an *analytic* family of examples that is relevant to observations how the complexity associated with variable liquid water and the geometry of clouds alone can fundamentally alter radiative transfer properties and, for instance, our inference of the thermal structure of atmospheres. In particular, effects due to the random variation

in optical depths associated with the complexity of clouds can be mistakenly interpreted in terms of the variation in the vertical temperature profile in the model atmosphere. Further, we will show how this might profoundly affect applications of radiative transfer theory, including climatic change.

2. Two-temperature cloud structure model

In order to show simply how randomness in cloud structure (which we associate with the usual "puffiness" observed in cumulus clouds) influences radiative transfer, consider a situation where we have two layers of material, one at temperature T_1 (and corresponding source function S_1) and an underlying layer at temperature T_2 (and corresponding source function S_2). We assume that the transition from one temperature to the next occurs at optical depth τ_0. Figure 2 illustrates this simple plane-parallel geometry, which is typical of conventional radiative transfer models that assume lateral homogeneity. Here, μ is the cosine of the emission angle, that is, the angle between the vertical and the line of sight.

The usual theory of radiative transfer (Chandrasekhar 1960) in an atmosphere can be written

$$\mu \frac{\partial I}{\partial \tau} = I(\tau, \mu) - S(\tau), \tag{1}$$

which can be expressed in integral form as

$$I(0, \mu) = \frac{1}{\mu} \int_0^\infty S(\tau) \exp\left(-\frac{\tau}{\mu}\right) d\tau. \tag{2}$$

Here τ is the optical depth at a given waveband, $I(\tau, \mu)$ is the observed intensity at $\cos^{-1}\mu$ at that optical depth, and $S(\tau)$ is the source function at that optical depth. This latter equation is particularly useful since it describes the intensity observed at the top of the atmosphere ($\tau = 0$), for example, from a spacecraft as a function of the viewing angle. For this reason, $I(0, \mu)$ is sometimes called the limb-darkening function (Newman and Sagan 1978). This equation can be formally inverted then to yield the source function as a function of optical depth, thereby providing insight into the temperature structure of the atmosphere.

Later, we will see that this latter expression can be related simply to a Laplace transformation. This is important since the computation of an inverse Laplace transform, unlike the inverse Fourier transform, is highly ill conditioned; this in turn magnifies any uncertainties in the source function or in the appropriateness of the plane-parallel model. Böhm (1961) showed that the above integral could be expressed in convolutional form, reducing the inversion problem to a deconvolution; this consequently magnifies any uncertainty in the high spatial frequency components of the source function. (Computationally, however, Böhm's observation is not useful, as one must resort to Fourier or Laplace methods to achieve the deconvolution.) We will proceed shortly to show that randomness in cloud shape introduces a fundamental modification of this expression, as well as an operational ill conditionedness in its inversion to obtain the temperature structure of an atmosphere.

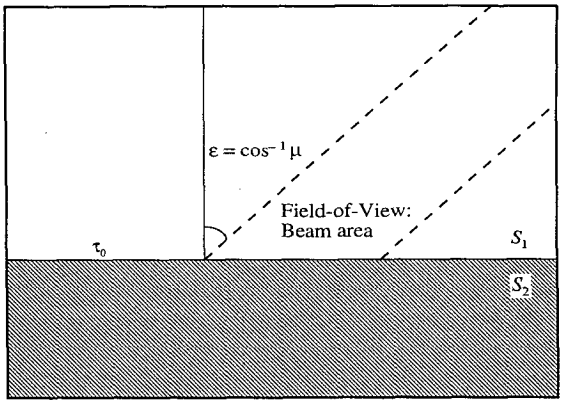

FIG. 2. Illustration of the usual two-layer model for radiative transfer. The optical depth of the interface is τ_0, while μ is the cosine of the emission angle.

In the case of the simple model above, we obtain

$$I(0, \mu) = S_1 + (S_2 - S_1) \exp\left(-\frac{\tau_0}{\mu}\right). \tag{3}$$

Assuming that $S_2 > S_1$, that is, that temperature increases with optical depth, we see that the intensity at the subsolar point is greater than that at the limb, an example of limb darkening—the usual situation where the intensity appears to diminish as one goes from the subsolar point to the limb.

Suppose, however, that we replace the idealization represented by Fig. 2 with one that contains a realistic description of the liquid water distribution, individual cloud geometry, and relative placement of clouds. The point here is that for a given light pencil, Eq. (3) remains valid so long as τ_0 is the optical depth of the interface measured *at the point* where the light pencil intersects the second cloud layer. What we observe with an instrument is a collection or *sampling* of light pencils each with the same emission angle but with different optical depths τ_0. Thus, we must average over the distribution of optical depths τ_0 that have been sampled. A more appropriate description for the intensity function is then

$$I(0, \mu) = S_1 + (S_2 - S_1) \int_0^\infty \exp\left(-\frac{\tau}{\mu}\right) f(\tau)\, d\tau, \tag{4}$$

where $f(\tau)\, d\tau$ describes the probability that the optical depth of the interface lies between τ and

$\tau + d\tau$. This general description can be adapted to the plane-parallel geometry case above by taking

$$f(\tau) = \delta(\tau - \tau_0), \tag{5}$$

where $\delta(x)$ is the Dirac delta function.

In Fig. 3, we plot the frequency histogram corresponding to the observational data in Fig. 1. This distribution corresponds directly to $f(\tau)$. It is approximately Gaussian but reveals significant skew and, of course, vanishes for $\tau < 0$. A better statistical description may be shown to have the form of a Gamma distribution, that is, a function of the form $\tau^n \exp(-\beta\tau)$, where n and β are determined by observations. For these data, we find that $n \approx 10$ and $\beta \approx 0.18$. This we will describe below. We will employ this functional form since it seems to better characterize the tails of the distribution, that is, $\tau \approx 0$ and $\tau \to \infty$. We will return to the question of the nature of the distribution function for the optical depth shortly.

Due to the fact that $\exp(-\tau/\mu)$ is a concave functional over a convex space, an elementary result in real analysis known as Jensen's inequality (Rudin 1966) applies. (A simple proof is provided in the appendix.) If we take τ_0 to be the mean value $\langle\tau\rangle$ of the distribution

$$\tau_0 = \langle\tau\rangle \equiv \int_0^\infty \tau f(\tau) d\tau, \tag{6}$$

then Jensen's inequality gives

$$\left\langle \exp\left(-\frac{\tau}{\mu}\right)\right\rangle \geqslant \exp\left(-\frac{\langle\tau\rangle}{\mu}\right). \tag{7}$$

Consequently, the observed intensity in (4) will *always* be greater than the intensity we would predict for the plane-parallel approximation given the same source function! Thus, we already see an indication of *systematic* effects appearing in the presence of complex cloud geometry. This inequality will be most pronounced when $\mu \approx 1$, that is, when we are looking straight down. Hence, as we interpret the limb-darkening function to be a line-of-sight integration of the source function, one outcome of this inequality is that we are qualitatively led to think that the source function is *always* greater than it actually is.

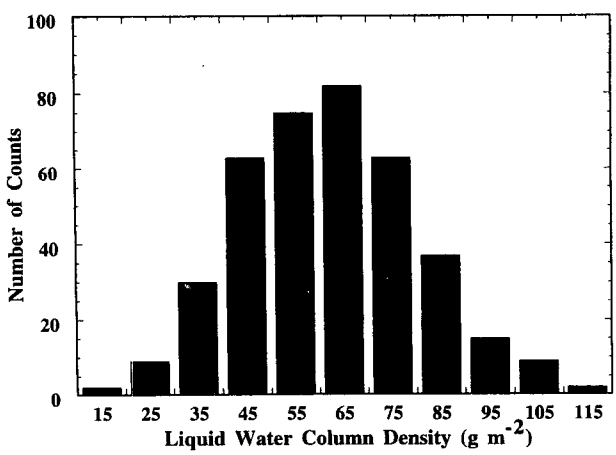

FIG. 3. Frequency histogram for data shown in Fig. 1. Note substantial width of the distribution and slight asymmetry.

The quintessential difference between this idealized plane-parallel case and the more realistic situations with which we are concerned is that this distribution function f has a peak, say, in the neighborhood of τ_0 but also has some *width*. (In the case of the observational data presented in Fig. 1, the width relative to the mean is $\sim$ 30%.) We will now show that the width of the distribution of optical depths substantially modifies the observed intensity. Further, if we assume that Eq. (3) is valid, then our inference of $S(\tau)$ will also be substantially broadened and, possibly, be qualitatively incorrect. Indeed, the observation due to Böhm implies that inaccuracy in the limb-darkening function can be substantially amplified.

In the next section, we consider a family of distribution functions, based upon the Gamma distribution (Feller 1968a,b), which in some limit converges to Eq. (5). We employ this distribution because it reproduces crudely some of the observed features of real clouds and because we can derive analytically results that are not prone to numerical errors and possible misinterpretation. Then we will show how it alters the observed intensity function and our inference of the source function and the atmosphere's vertical temperature structure.

3. Gamma distribution

The Gamma distribution employed in probability theory (Feller 1968a,b) is given by

$$p_n(x) \equiv \frac{x^n}{n!} \exp(-x), \tag{8}$$

which peaks at $x = n$ and has the mean value

$$\langle x\rangle \equiv \int_0^\infty x\, p_n(x)\, dx = n + 1, \tag{9}$$

and variance

$$\left\langle [x - \langle x\rangle]^2 \right\rangle = \langle x^2\rangle - \langle x\rangle^2 = n + 1. \tag{10}$$

The Gamma distribution is a continuous function of x and is intimately related to Poisson processes and, especially, to the sum of n -independent exponentially distributed random variables (Feller 1968a,b).

It is useful to rescale this class of distribution functions so that their peak values are the same. We define a family of probability distributions $q_n(x)$ according to

$$q_n(x) \equiv \frac{\beta_n}{n!} (\beta_n x)^n \exp(-\beta_n x), \tag{11}$$

where the quantity $\beta_n > 0$ is yet to be defined. We trivially observe that the peak value is situated at n/β_n. Thus, it is convenient to select β_n so that the mean of the distributions, say τ_0, is independent of n, that is, according to

$$\beta_n = \frac{n+1}{\tau_0}. \tag{12}$$

Accordingly, we find that the family of distribution functions $q_n(x)$ satisfies

$$\langle x \rangle = \tau_0, \tag{13}$$

and

$$\left\langle [x - \langle x \rangle]^2 \right\rangle = \frac{\tau_0^2}{n+1}. \tag{14}$$

Finally, it follows that

$$\lim_{n\to\infty} q_n(x) = \delta(\tau - \tau_0), \tag{15}$$

since

$$\int_0^\infty q_n(\tau)\, d\tau = 1, \tag{16}$$

and, for $\tau \neq \tau_0$,

$$\lim_{n\to\infty} q_n(\tau) = 0. \tag{17}$$

By applying Eqs. (13) and (14) to the data in Fig. 1, we obtain that $n = 10.61 \approx 10$ and that $\beta \approx 0.18$. (Given the probabilistic basis for the Gamma distribution, this result provides a hint that there were on average approximately ten "events" or substructures associated with the line of sight.) In Fig. 4, we plot the cumulative distribution function for the 387 data points in Fig. 1 against the corresponding liquid water column density (dotted line). The solid line is the two-parameter (n and β) Gamma distribution estimate to this distribution function. The degree of agreement between the observed and empirically fitted distribution functions is particularly good. The reliability of this fit is further confirmed in Fig. 5, where (for every value of the liquid water column density) the cumulative probability for the data point is plotted against its Gamma distribution fit. Ideally, this should be a straight line proceeding from the origin to the point (1, 1)—the quality of the fit is evident. (We also explored a Gaussian distribution and considered the equivalent "normal probability plot." The agreement was not as good, owing to the skew in the original data. Nevertheless, there was substantial similarity in the fit distribution—a reflection of the fact that for large n a gamma distribution becomes asymptotically Gaussian.) These insights gained from the Gamma distribution and its value in fitting real data can be employed in a practical way. By using the mean *and* the variance (or standard deviation) of the optical depth, we can obtain a useful fit to its distribution function—certainly better than the Dirac δ function implicitly employed by standard methods—which can be used now in the inversion of data.

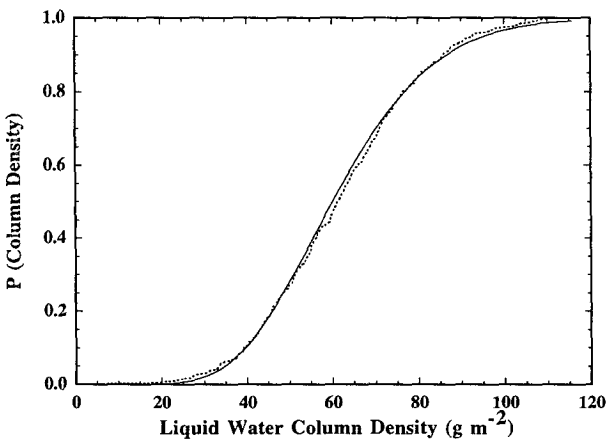

FIG. 4. Cumulative distribution function for liquid water column density in Fig. 1 (dotted line) and corresponding Gamma distribution function $n = 10$ fit.

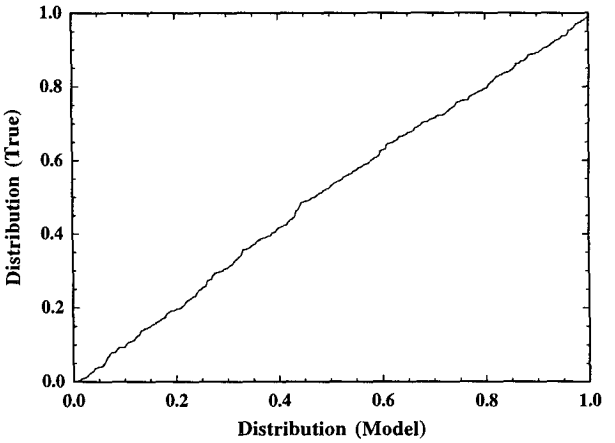

FIG. 5. Probability plot for Fig. 1 with Gamma $n = 10$ model: cumulative distribution for observations plotted against cumulative distribution for Gamma distributon fit. Plot shows that data can be described very accurately by the functional form $\tau^n \exp(-\beta\tau)$.

4. Limb-darkening function

Given this definition, we obtain for the limb-darkening function (4), appropriate to a cloud layer whose optical depth at the interface is distributed according to $q_n(\tau)$, that

$$I_n(0,\mu) = S_1 + \frac{S_2 - S_1}{\left(1 + \frac{\tau_0}{\mu}\frac{1}{n+1}\right)^{n+1}}, \tag{18}$$

where we have introduced a subscript n to indicate that we are dealing with the distribution function $q_n(\tau)$. (In principle, we should employ the mean value operator $\langle \cdots \rangle$ around the intensity; we do not do so

for notational simplicity.) Note in the limit $n \to \infty$ we recover the usual expression (3). Intuitively, the limb-darkening function is interpreted as a measure of the temperature at the optical depth from where most of the integrated intensity comes, that is, for $\tau \approx 1$ for $\mu = 1$ (zenith) and the top of the atmosphere for μ small (limb). As pointed out earlier, we observe that the intensity associated with distribution functions with nonvanishing widths are *systematically* greater than the ideal plane-parallel case. Hence, this trend leads to exaggerated estimates of temperature at depth!

We wish to see how this limb-darkening function varies for $\tau_0 = 1$ for different values of n and how that compares with the ideal plane-parallel case, that is, $n \to \infty$. In Fig. 6, we show how the intensity varies with the cosine of the emission angle for $\tau_0 = 1$, as a typical case of the limb-darkening function. We display the limb-darkening function according to $n = 1, 3, 10$ as well as ∞. (Note that $n = 10$ corresponds closely to the data in Fig. 1.) The most prominent feature here is how broad the intensity as a function of emission angle has become for the smaller values of n. We wish to see now how this broadening or smoothing in the observed intensity influences our inference of the source function and of the vertical temperature profile.

5. Source function

From an observational viewpoint, the relevant question to ask is given an observed intensity function, what is the associated source function? If a plane-parallel model were appropriate, we would wish to employ Eq. (2). To convert this into the canonical problem of inverting a Laplace transform, define $\mathcal{J}(\nu)$ by

$$\mathcal{J}(\nu) \equiv \mu\, I(0, \mu), \tag{19}$$

where

$$\nu \equiv \frac{1}{\mu}. \tag{20}$$

Then, we have that

$$\mathcal{J}(\nu) = \int_0^\infty S(\tau) \exp(-\tau\nu)\, d\tau, \tag{21}$$

which has a formal inverse (assuming that we can analytically continue the intensity in the complex ν plane) given by the Bromwich integral

$$S(\tau) = \frac{1}{2\pi i} \int \mathcal{J}(\nu) \exp(+\tau\nu)\, d\nu, \tag{22}$$

where the integral is performed around the usual contour containing the origin.

Thus, we obtain for the example at hand that

$$S(\tau) = \frac{1}{2\pi i} \int \left[\frac{S_1}{\nu} + \frac{(S_2 - S_1)\beta_n^{n+1}}{\nu\ (\beta_n + \nu)^{n+1}} \right] \times \exp(+\tau\nu)\, d\nu. \tag{23}$$

Straightforward but tedious algebra yields that

$$S(\tau) = S_1 + (-)^n \frac{(S_2 - S_1)\beta_n^{n+1}}{n!} \frac{d^n}{d\beta_n^n} \times \left\{ \frac{1}{\beta_n} [1 - \exp(-\tau\beta_n)] \right\}. \tag{24}$$

More manipulation yields

$$S(\tau) = S_1 + (S_2 - S_1) \times \left[1 - \exp(-\tau\beta_n) \sum_{m=0}^{n} \frac{(\beta_n\tau)^m}{m!} \right], \tag{25}$$

where we continue to employ $\beta_n = (n + 1)/\tau_0$.

It is easy to show that the bracketed quantity asymptotically approaches a Heaviside function in $\tau - \tau_0$ as $n \to \infty$. The quantity in brackets is always positive, and the summation approaches $\exp(\beta_n\tau)$ as $\beta_n\tau \to 0$. Hence, for small values of $\beta_n\tau$, the term in brackets vanishes. For large values of $\beta_n\tau$, the exponential term dominates over the algebraic sum, and the bracketed quantity approaches unity. To complete the proof, it is sufficient to show that the derivative of the bracketed quantity has the character, in the limit $n \to \infty$ of a Dirac δ function; that is, it is nonnegative and vanishes away from $\tau = \tau_0$. (We have already established that it satisfies the unit integral requirement.) Some simple algebra shows that the derivative of the bracketed quantity is

$$\exp(-\beta_n\tau) \frac{(\beta_n\tau)^n}{n!}, \tag{26}$$

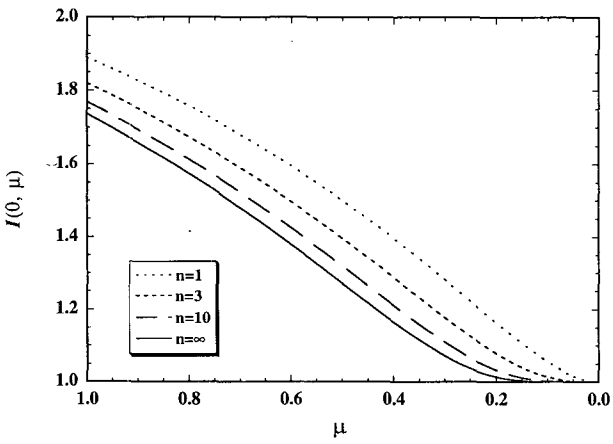

FIG. 6. Intensity at top of atmosphere $I(0, \mu)$ as a function of the cosine of the emission angle μ for $\tau_0 = 1$. The solid curve corresponds to the plane-parallel result (3), while the dashed curves correspond to different values of n in the model (18). Here $S_2/S_1 = 2$.

which is nonnegative and is maximized when

$$\beta_n \tau = n \quad \text{or} \quad \tau = \frac{n}{n+1}\tau_0.$$

Away from the maximum, this quantity goes to zero and at maximum is $O(\sqrt{n})$, thus completing the proof. Employing (12), we see that the width of the distribution goes as $1/\sqrt{n+1}$, which establishes that $S(\tau)$ systematically converges in some sense to a Heaviside function.

In Fig. 7 we plot this inferred distribution for a variety of cases specified by $n = 0, 1, 3, 10, \ldots, \infty$ and with $\tau_0 = 1$. This figure shows behavior quite different from a step function. What is particularly clear from this figure is that we have effectively reassigned the width of the optical depth distribution to that of the temperature distribution owing to the inadequacies of the plane-parallel model. (Quantitatively, the width here is visually substantially greater than the width associated with the relevant distribution function.) The sensitivity of the inverse Laplace transform to any variation in the quantity to be transformed has effectively amplified the uncertainties in the intensity distribution to give us this anomalous estimate of the source function. Qualitatively, we see that the randomness in the position of the interface will be misinterpreted as a slower rate of temperature change as one goes to greater optical depths.

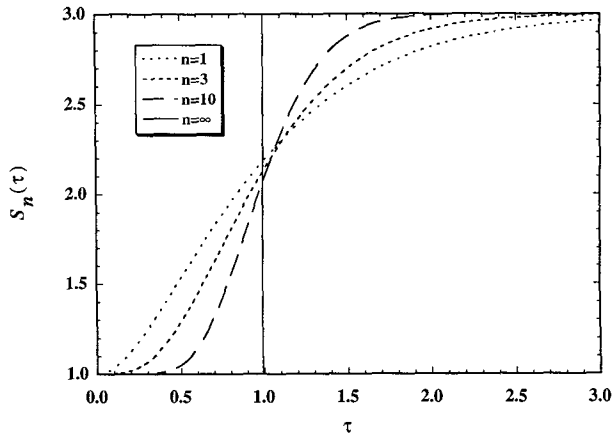

FIG. 7. For case of $\tau_0 = 1$, plot of the source function for $n = 1, 3, 10, \infty$. Note that the source function is artificially broadened, particularly for smaller values of n.

6. Conclusions

We have learned in recent years that the description of the optical depth of the atmosphere is strongly dependent upon the highly variable liquid water content, morphology, and placement of clouds. We have considered a particularly simple physical model that does not include multiple scattering events yet accurately describes the statistics of the integrated water vapor content of real clouds. We have argued here that *any* form of physical and/or geometrical complexity will translate into optical pathlengths that vary randomly, and that observations will generally correspond to spatial averages over this distribution of optical depths. As a specific example, we considered the intensity of radiation emerging from the top of an atmosphere (as in limb intensity observations made by satellites) as a function of the emission angle. There we found that a substantial quantitative change in the intensity would result from a random distribution of cloud thicknesses. Consequently, we then showed that our inference of the temperature structure of the cloud deck (as seen through its source function) would depart substantially from the true one. A variability of the order of 30% as observed in Fig. 1 in the optical depth readily translates into a 3%–5% error in the inferred limb-darkening function (Fig. 6) and a substantial uncertainty—as much as several degrees, more than prevailing uncertainties generally associated with the greenhouse model—in temperature (Fig. 7).

Since the temperature as a function of height is fundamental to many meteorological and climatological considerations (e.g., computation of opacities, the determination of the altitude where water vapor saturation occurs, etc.), this effect can substantially influence our *quantitative* understanding of atmospheric structure. This in turn could have a major effect on questions having to do with the greenhouse effect and global warming, as we are dealing there with small differences between rather large numbers, including quantities associated with irradiance, opacity, etc. Nevertheless, these small differences have a large impact. It is noteworthy that we have explored but one example (via the limb-intensity function) of how complex cloud geometries can lead to physical misinterpretation. Our specific examples were selected to be of generic interest, as well as analytic, revealing how plane-parallel geometry can be regarded as a special case of a more realistic distribution. With these results in hand, it follows that we must carefully reconsider how the geometry of clouds should be introduced into our modeling of weather and of climate.

We have used the Gamma distribution to represent the randomness in the distribution of optical pathlengths, as well as some powerful results from functional analysis, because they permit the evaluation of analytic results that effectively illustrate the effects of randomness in the inversion of temperature profiles from remote sensing measurements. Physical processes (e.g., nonuniform chemical composition as well as spatial and temporal variability in liquid water content) are forms of inhomogeneity that can erroneously influence inferences made regarding radiative transfer and the greenhouse effect. Finally, we have identified a simple procedure for characterizing the underlying randomness—through the mean and

standard deviation and their corresponding Gamma distribution—from which we can obtain a more accurate estimate of the underlying atmospheric temperature structure.

Acknowledgments. We wish to thank R. Turco, D. Levermore, and C. Sagan for several interesting discussions. One of the authors (JKL) was partially supported by NASA Grant NAG1-1126. Part of this work was supported by NSF ATM-9216646.

APPENDIX

Jensen's Inequality for Radiative Transfer

A simple proof of Jensen's inequality applied to radiative transfer, namely,

$$\left\langle \exp\left(-\frac{\tau}{\mu}\right)\right\rangle \geq \exp\left(-\frac{\langle\tau\rangle}{\mu}\right),$$

emerges from considering the Taylor series with remainder (Apostol 1967). Assume that f has continuous derivative of order $n+1$ in some interval containing X. Then, for every x in this interval, we have the Taylor formula with remainder

$$f(x) = \sum_{k=0}^{n} \frac{f^{(k)}(X)}{k!}(x-X)^k + E_n(x), \qquad \text{(A1)}$$

where

$$E_n(x) = \frac{1}{n!}\int_X^x (x-t)^n f^{(n+1)}(t)dt. \qquad \text{(A2)}$$

The proof follows by induction by repeated integration by parts. An especially relevant case emerges when $n = 1$, whereupon we find

$$f(x) = f(X) + f'(X)(x-X) + E_1(x), \qquad \text{(A3)}$$

where

$$E_1(x) = \int_X^x (x-t)f''(t)dt. \qquad \text{(A4)}$$

This expression can be verified immediately by integration by parts.

Suppose that x is a random variable on some domain D with distribution $P(x)$ and whose mean

$$X \equiv \int_D x dP(x) \qquad \text{(A5)}$$

exists. Suppose, further, that $f''(x) \geq 0$ in D; this happens to be true for $\exp(-x)$, which is ubiquitous in radiative transfer. Moreover, it is simple to show that $E_1(x) \geq 0$. Then, we note that

$$\begin{aligned}\int_D f(x)dP(x) - f(X) &= \int_D \left[f(X) + f'(X)(x-X) + E_1(x)\right] dP(x) - f(X)\\ &= f(X) + f'(X)(X-X) + \int_D E_1(x)dP(x) - f(X)\\ &= \int_D E_1(x)dP(x) \geq 0, \qquad \text{(A6)}\end{aligned}$$

thereby proving our basic result. Hence, the average of the (exponential) function is strictly greater than the function of the average.

REFERENCES

Apostol, T. M., 1967: *Calculus*. Vol. 1. Blaisdell, 666 pp.

Barker, H. W., 1993: Radiative transfer through clouds possessing isotropic variable extinction coefficient. *Quart. J. Roy. Meteor. Soc.*, **118**, 1145–1162.

Böhm, K. H., 1961: A basic limit of the information contained in center-to-limb observations. *Astrophys. J.*, **134**, 264–267.

Bretherton, C. S., 1990: A multifractal model of entrainment into a stratocumulus cloud top. *Conf. on Cloud Physics*, San Francisco, CA, Amer. Meteor. Soc., 43–47.

Cahalan, R. F., 1989: Overview of fractal clouds. *Advances in Remote Sensing Retrieval Methods (RSRM '87)*, A. Deepak, H. E. Fleming, and J. S. Theon, Eds., A. Deepak Publishing, 371–389.

Carter, E. W., and G. L. Siscoe, 1987: The study of cumulus clouds as fractals. *UCLA Undergraduate Science Journal*, **4**, 19–24.

Chandrasekhar, S., 1960: *Radiative Transfer*. Dover, 393 pp.

Cotton, W. R., and R. A. Anthes, 1989: *Storm and Cloud Dynamics*. Academic Press, 883 pp.

Davis, A., P. Gabriel, S. Lovejoy, D. Schertzer, and G.L. Austin, 1990: Discrete angle radiative transfer—Part III, Numerical results and meteorological applications. *J. Geophys. Res.*, **95**, 11 729–11 742.

——, S. Lovejoy, and D. Schertzer, 1991a: Discrete angle radiative transfer in a multifractal medium. *SPIE Proc.*, **1558**, 37–59.

——, ——, and ——, 1991b: Radiative transfer in multifractal clouds. *Scaling, Fractals and Non-linear Variability in Geophysics*, D. Schertzer and S. Lovejoy, Eds., Kluwer, 303–318.

Evans, K. F., 1993: A general solution for stochastic radiative transfer. *Geophys. Res. Lett.*, **20**, 2075–2078.

Feller, W., 1968a: *An Introduction to Probability Theory and Its Applications*. Vol. 1. 3d ed. John Wiley, 153–159.

——, 1968b: *An Introduction to Probability Theory and Its Applications*. Vol. 2. 2d ed. John Wiley, 47–48.

Hentschel, H. G. E., and I. Procaccia, 1984: Relative diffusion in turbulent media: The fractal dimension of clouds. *Phys. Rev. A*, **29**, 1461–1470.

Heymsfield, A. J., and D. J. Musil, 1982: The 22 July 1976 case study: Storm structure deduced from penetrating aircraft. *Hailstorms of the Central High Plains*, Vol. II. C.A. Knight and P. Squires, Eds., Colorado Associated University Press, Boulder, 163–180.

Houghton, J. T., 1988: *The Physics of Atmospheres*. 2nd ed. Cambridge University Press.

Johnson, D. S., 1957: Trade wind cloud measurements windward of the island of Hawaii. *Tellus*, **9**, 495–508.

Lovejoy, S., 1982: Area-perimeter relation for rain and cloud areas. *Science*, **216**, 185–187.

Mandelbrot, B. B., 1988: People and events behind the science of fractal images. *The Science of Fractal Images*, H. O. Peitgen and D. Saupe, Eds., Springer-Verlag, p. 13.

Newman, W. I., and C. Sagan, 1978: Five micron limb-darkening and the structure of the Jovian atmosphere. *Icarus,* **36**, 223–239.

Pomraning, G. C., 1991: *Linear Kinetic Theory and Particle Transport in Stochastic Mixtures*. World Scientific Publishing, 235 pp.

Rogers, R. R., and M. K. Yau, 1989: *A Short Course in Cloud Physics*. 3rd ed., Pergamon Press, 293 pp.

Rudin, W., 1966: *Real and Complex Analysis*. McGraw-Hill, p. 61.

Slingo, A., R. Brown, and C. L. Wrench, 1982: A field study of nocturnal stratocumulus; III. High resolution radiative and microphysical observations. *Quart. J. Roy. Meteor. Soc.*, **108**, 145–165.

Squires, P., and J. Warner, 1957: Some measurements in the orographic cloud of the island of Hawaii and in trade wind cumuli. *Tellus*, **9**, 475–494.

Stephens, G. L., 1988a: Radiative transfer through arbitrarily shaped media–Part 1: General theory. *J. Atmos. Sci.*, **45**, 1818–1836.

——, 1988b: Radiative transfer through arbitrarily shaped media–Part 2: Closures. *J. Atmos. Sci.*, **45**, 1837–1848.

——, P. M. Gabriel, and S.-C. Tsay, 1991: Statistical radiative transport in one-dimensional media and its application to the terrestrial atmosphere. *Trans. Theory and Stat. Phys.*, **20**, 139–175.

Telford, J. W., and P. B. Wagner, 1981: Observations of condensation growth determined by entity type mixing. *Pure Appl. Geophys.*, **119**, 934–956.

Warner, J., 1969: The microstructure of cumulus cloud. Part I. General features of the droplet spectrum. *J. Atmos. Sci.*, **26**, 1049–1059.